

Contents lists available at ScienceDirect

International Journal of Mass Spectrometry

journal homepage: www.elsevier.com/locate/ijms



Structure-elucidation of human CCL5 by integrating trapped ion mobility spectrometry-mass spectrometry (TIMS-MS) with Structure Relaxation Approximation (SRA) analysis



Mengqi Chai a, Christian Bleiholder a, b, *

- ^a Department of Chemistry and Biochemistry, Florida State University, 95 Chieftan Way, Tallahassee, FL, 32306-4390, USA
- b Institute of Molecular Biophysics, Florida State University, 91 Chieftan Way, Tallahassee, FL, 32306-4390, USA

ARTICLE INFO

Article history: Received 23 April 2021 Received in revised form 4 August 2021 Accepted 6 August 2021 Available online 10 August 2021

Keywords: Trapped ion mobility spectrometry Structure relaxation approximation Chemokine C-C motif Ligand 5

ABSTRACT

Ion mobility spectrometry-mass spectrometry offers the potential to characterize structures of transient protein assemblies and protein isoforms by means of their orientationally-averaged momentum transfer cross-sections. A commonly observed phenomenon is the compaction of a protein in the ion mobility measurement, that is, the cross section measured for the protein by ion mobility spectrometry is smaller than the cross section expected for its native structure. Consequently, this compaction means that at least some structural changes of the protein must have occurred during the ion mobility measurement. A major challenge is then to identify which aspects of the solution structure are retained in the ion mobility measurement and which ones are not. Here, we apply our recently developed Structure Relaxation Approximation (SRA) method in conjunction with trapped ion mobility spectrometry-mass spectrometry (TIMS-MS) to probe compaction of the human protein chemokine (C-C motif) ligand 5 (also CCL5). Ion mobility spectra are recorded for various charge states and solution conditions of CCL5 under both "soft" and collisionally-activated conditions. Our data show that the SRA reproduces the overall trends in the experimental spectra: (1) the compaction of the CCL5 structure as seen in the experiments; (2) the general increase in the cross section for the various charge states; and (3) the increase in cross section after collisional-activation. The SRA attributes the compaction of the CCL5 structure mainly to the folding of the unstructured N-terminus onto the central Greek key motif of CCL5. By contrast, the SRA indicates that native residue-residue contacts present in the NMR structure are largely retained. Additionally, our analysis indicates that accurate treatment of proton transfer processes during the structural relaxation process would significantly improve the structural interpretation of ion mobility data by the SRA.

© 2021 Published by Elsevier B.V.

1. Introduction

The function of a protein is intimately linked to the structures it adopts and to the motions by which they interconvert [1,2]. Thus, traditional biophysical methods are invaluable for pharmaceutical research by providing structural details about proteins involved in human diseases [3].

Proteins are complex entities, however, and currently existing biophysical methods are limited in what aspects of protein structures can be revealed. One limitation arises from presence of coexisting, transiently populated species, such as the amyloid- β

assemblies implicated in Alzheimer's disease [4]. Another limitation arises from the co-existence of proteoforms, differentially modified variants of the same protein [5]. Glycoforms of glycoproteins, protein variants that differ in the structure and sequence of their glycans, are of particular current relevance because viral spike proteins are often heavily and heterogeneously glycosylated [6,7].

Ion mobility spectrometry-mass spectrometry (IMS-MS) offers the potential to characterize structures of transient protein assemblies [8,9] or protein variants including glycoforms [10,11]. Nevertheless, a key challenge in applying IMS-MS to protein structure characterization is that IMS-MS is not a "structure method" in the same sense that, for example, X-ray crystallography or nuclear magnetic resonance (NMR) spectroscopy both are. Whereas the X-ray diffraction pattern is directly related to the

^{*} Corresponding author. Department of Chemistry and Biochemistry, Florida State University, 95 Chieftan Way, Tallahassee, FL, 32306-4390, USA. E-mail address: cbleiholder@fsu.edu (C. Bleiholder).

atomic structure of the molecule [12], and NMR spectroscopy directly yields interatomic distances and angles within a molecule [13], IMS-MS provides no such direct, atomic information about the molecule under investigation. In fact, IMS-MS convolves the entire protein structure into a mean "effective area", where the mean is taken over all orientations and all conformations of the protein samples during the measurement. This effective area is the orientationally-averaged momentum transfer cross-section of the ion. The challenge, thus, is to identify as many aspects as possible about the atomic structure of the ion from its momentum transfer cross-section.

The structural interpretation of the measured cross section is challenging largely because the ion mobility experiment is not an equilibrium measurement [14–16]. One commonly observed phenomenon is the compaction of the protein in the ion mobility spectrometer [17–23]. This means that the experimentally determined cross section is significantly lower than the cross section expected for the X-ray or NMR structures. A compaction is often reported for proteins with flexible linker or hinge regions such as antibodies and other non-globular proteins [24].

We recently developed the Structure Relaxation Approximation (SRA) method to structurally interpret ion mobility spectra [16]. The central aspect of the SRA is to predict charge-state specific ion mobility spectra for a protein system. To this end, the SRA considers the structural relaxation process that a native solution structure would undergo during the ion mobility measurement in the gas phase after removal of solvent. The idea is then that the more charge states and experimental conditions are probed by experiment and theory, the greater the confidence of the structural interpretation of the ion mobility data because chance agreement for all conditions becomes increasingly unlikely.

Equally important, however, is that discrepancies between the experiment and the SRA predictions enable the analyst to identify and improve shortcomings in the theoretical analysis of the IMS data, thereby successively advancing the understanding of gas phase dynamics occurring in protein systems during ion mobility measurements. By contrast, and as discussed [16], no such improvement can result from efforts rationalizing ion mobility measurements through seeking agreement between theory and experiment.

In our original formulation of the SRA, we probed how closely, and in which aspects, ions of the protein ubiquitin detected by "soft" ion mobility measurements resemble the native state [16]. The SRA predicted that ubiquitin retains essentially the same residue-residue contacts as the native state determined by X-ray crystallography when measured by "soft" ion mobility methods. We were able to draw these conclusions because we varied solution conditions and, using a home-built tandem-TIMS instrument [25,26], we conducted charge-reduction experiments for selected charge states of ubiquitin. Additionally, we were able to utilize the equivalent data measured in a different buffer gas based on data reported by other groups [14,27]. Equivalent data are not commonly available, however, which renders it unclear how widely applicable the SRA method is to study protein structures in conjunction with commercially available ion mobility spectrometry/mass spectrometry instruments. Further, it is unclear how well the SRA would perform in describing the compaction of a protein.

A common and widely available approach to characterize the structure of a protein using ion mobility spectrometry — mass spectrometry methods is collision-induced unfolding (CIU) [28,29]. Hence, here, we probe how well the SRA assesses protein structures using collisional-activation experiments. Additionally, we conduct the measurements using TIMS-MS instead of tandem-TIMS-MS, because this setup is equivalent to IMS-MS instruments that are widely available. Hence, the approach discussed here can be carried

out using commercial instruments.

Specifically, we apply the SRA method to probe the structure of the chemokine CCL5. Chemokines are an important class of cytokines involved in many biological processes, including inflammation, wound healing, lymphoid trafficking [30]. CCL5, also known as RANTES (regulated on activation, normal T cell expressed and secreted), is a CC-type chemokine containing two adjacent cysteines at positions 10 and 11 that form disulfide bonds with cysteines at positions 34 and 50, respectively. CCL5 mediates cell migration in vivo, T cell activation and apoptosis [31–33]. CCL5 is also a potential HIV inhibitor as its receptor CCR5 is the coreceptor of the CD4 receptor used by HIV to enter T cells and monocytes [34,35].

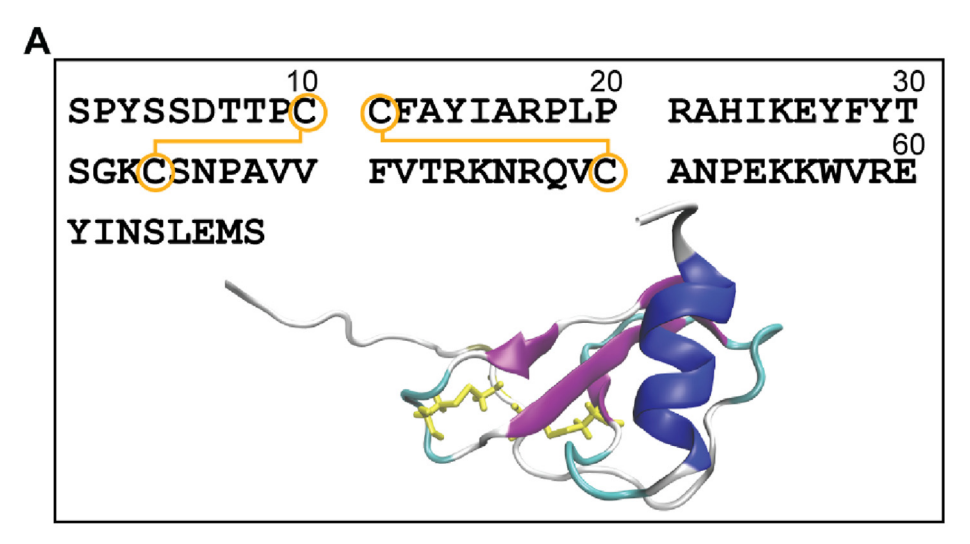
2. Experimental and computational details

2.1. Materials and sample preparations

CCL5 was purchased from PeproTech, Inc. (Rocky Hill, NJ). Ammonium acetate salt was purchased from Fisher Scientific International, Inc. (Hampton, NH). Water, formic acid, and acetonitrile were of LC/MS grade quality (Sigma-Aldrich). Dithiothreitol (DTT) was purchased from Sigma-Aldrich. A 200 mM stock solution of ammonium acetate with pH ~6 was prepared by dissolving 154 mg ammonium acetate powder into 2 mL of water. A 10 μM stock solution of CCL5 was prepared by adding 256 μ L of water to a sample vial containing 20 µg of CCL5. Solutions of CCL5 under three different conditions (ammonium acetate/native, aqueous solution, and reducing/denatured) were prepared for TIMS-MS measurements. The native solution (2 µM CCL5 in 10 mM ammonium acetate, pH 6) was prepared by diluting the stock CCL5 (10 µM in water) using appropriate amount of water and stock solution of ammonium acetate (200 mM). The aqueous solution (1 μ M in water) was prepared by diluting the stock CCL5 (10 µM in water) with water. To reduce the disulfide-bonds and denature CCL5, a solution with 2 μM CCL5 and 5 mM ammonium acetate was prepared using the stock solution. The 2 μ M CCL5 solution was then treated with DTT (1 mM) at 70 °C for 30 min. Subsequently, the solution was cooled over ice to 4 °C and acetonitrile and formic acid were added to the protein sample to a final concentration of 50 % and 1 % v/v, respectively, prior to mass analysis [36].

2.2. TIMS-MS instrumentation and measurements

All measurements were performed on a prototype ESI-TIMS-QqTOF mass spectrometer (Bruker Daltonics, Billerica, MA) as shown in Fig. S1 (Supplementary Data) and described in detail elsewhere [37–39]. Samples were infused at a rate of 180 μ L/h into the electrospray ion source with the desolvation gas temperature set to 304 K. The electrospray capillary voltage was set to 2.5-2.8 kV. An RF peak-to-peak voltage of 180 V was applied to each section to confine ions radially in the funnel regions and inside the TIMS tunnel. As described [40], high RF and DC potentials across the components of the TIMS device should be avoided because they promote denaturation of the protein structure during the measurement. To preserve native-like conformations, we thus applied "soft" operating settings as described [40]. As discussed [41], the DC potentials prior to mobility separation in the TIMS tunnel are crucial to conducting "soft" measurements; we hence applied 10 V between the deflector and the first plate of the entrance funnel and 20 V DC potential differences across the entrance funnel in accord with prior work. For collision-induced unfolding measurements, we employed "harsh" conditions that denature the protein structure. To this end, we applied a DC potential difference between the deflector and the first plate of the entrance funnel of 68 V and 292 V across the entrance funnel. For all ion mobility measurements, the



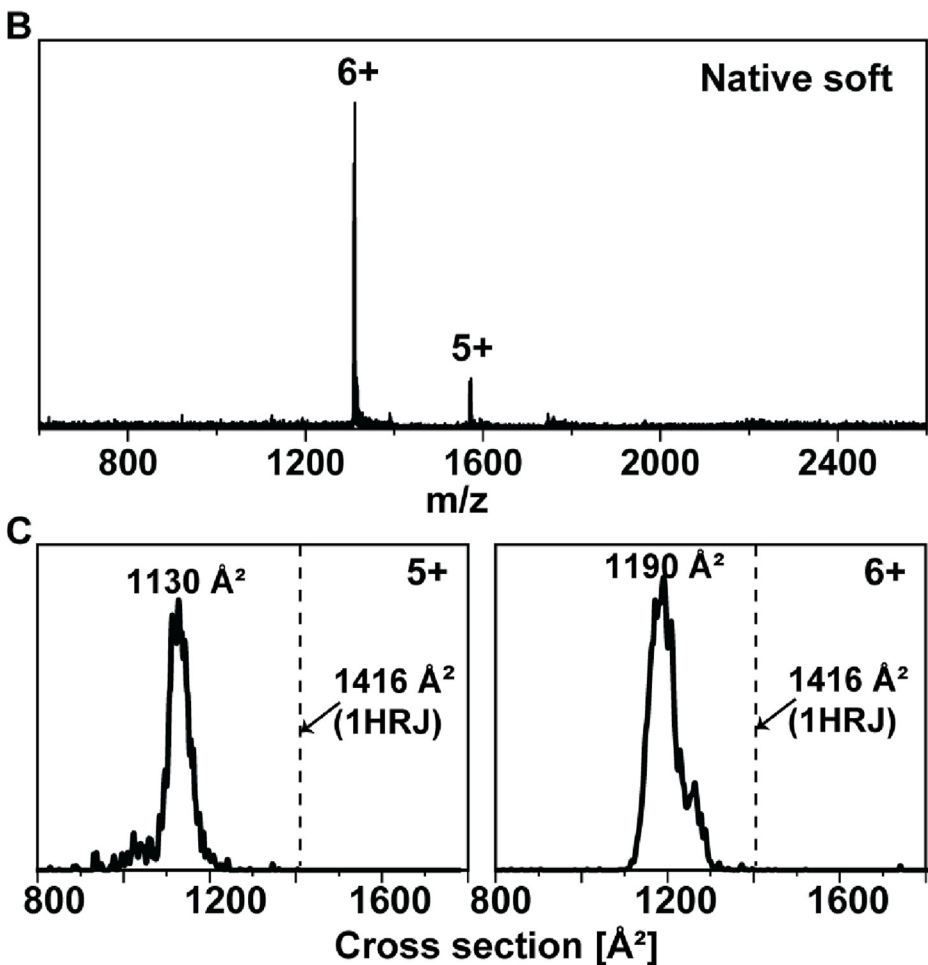


Fig. 1. Native TIMS-MS analysis of CCL5. (A) Amino acid sequence and NMR structure of CCL5 (PDB code: 1HRJ, monoisotopic mass is 7841.83 Da). Two disulfide bonds pair Cys10 with Cys34 and Cys11 with Cys50. (B) Native mass spectrum shows presence of charge states 5+ and 6+. (C) Ion mobility spectra for charge states 5+ and 6+ reveal a dominant feature with cross sections corresponding to 1130 Å^2 and 1190 Å^2 , respectively. The cross section of the NMR structure is calculated to 1416 Å^2 by the PSA method.

potential at the entrance of the TIMS tunnel was increased from -200 V to +10 V at a rate of $\beta=2.92 \text{ V/ms}$. The pressure in proximity to the entrance of the TIMS tunnel was maintained at 2.75 mbar. For each TIMS cycle, ions were accumulated for 13.68 ms prior to separation and ion mobility separation was carried out over 72 ms.

2.3. Calibration of momentum transfer cross sections

Ion mobilities and cross sections in TIMS are determined via a calibration procedure [37,38,42]. For calibration, we used phosphazenes contained in Agilent ESI tuning mix as calibrants as described elsewhere [41–44]. The reduced ion mobilities for

calibration were taken from a previous report [42] based on the cross sections reported by Stow el at [45]. Each spectrum was calibrated immediately after acquisition under identical operating settings.

2.4. Structure Relaxation Approximation (SRA) calculations

Structure relaxation approximation (SRA) calculations were carried out as described [16]. Initial structures for CCL5 were taken from the protein data bank (PDB: 1HRJ) [46]. For each of the monomer structures present in the entry, explicit-solvent molecular dynamics calculations were carried out with GROMACS [47] in conjunction with the amber ff03 force field [48] as described. The two disulfide bonds (Cys10-Cys34 and Cys11-Cys50) were kept intact for the aqueous simulations whereas reducing conditions were mimicked by breaking the disulfide bonds. The gas-phase relaxation of solution structures was carried out as described [16]; briefly, the experimental charge states were attained by (de) protonating residues based on their solvent accessibility and atomic partial charges. To predict spectra for the "soft" measurement settings, the subsequent gas phase molecular dynamics simulations were carried out as described [16]. This is based on the fact that the RF and DC voltages in the experiment were chosen comparable to those used in our previous studies [16,25,40] and that hence the effective temperatures of the CCL5 ions are approximately the same as those of the ubiquitin ions in our prior report. To predict spectra for the "harsh" settings in our experiments, we increased the duration of each heating step to 500 ps and increased the maximum temperature of the heating cycle to 900 K prior to cooling down to 300 K in steps of 100 K. This protocol was deemed appropriate because visual inspection revealed prevalence of fully unfolded and unstructured CCL5 species during the equilibration cycle at 900 K. We used the Projection Superposition Approximation (PSA) method to calculate cross sections as described [16,49-52].

3. Results and discussion

3.1. Native TIMS-MS spectra reveal compaction of CCL5

Fig. 1A shows the NMR structure of CCL5, composed of a disordered N-terminal loop followed by a 3_{10} -helix, three antiparallel β sheet arranged in a Greek key motif, and a C-terminal α -helix. CCL5 possesses two disulfide bonds (Cys10-Cys34; Cys11-Cys50) as shown in the Figure. Fig. 1B shows the mass spectrum recorded for CCL5 under native mass spectrometry conditions as described under Experimental Details. Charge state 6+ predominates the spectrum with minor abundance of charge state 5+. The corresponding ion mobility spectra are given in Fig. 1C. Both spectra reveal a dominant feature with cross sections of 1130 $Å^2$ and 1190 $Å^2$, respectively. Overall, these results are in line with prior ion mobility spectrometry/mass spectrometry measurements in the sense that (1) the native mass spectrum shows a small number of charge states; and that (2) the corresponding cross sections are similar in value to each other and indicate predominance of compact, folded structures.

The PSA method estimates the cross section for the NMR structure of CCL5 (PDB code:1HRJ) to 1416 Å², which is approximately 20 % larger than the cross sections measured in the experiment. Consistent with prior reports [17–23], such large deviations indicate that a significant "compaction" of the native CCL5 structure occurred during the ion mobility spectrometry measurement.

This compaction highlights the challenge faced when interpreting ion mobility data in terms of the protein structure: it is obvious from the data that some structural changes must have

occurred to the CCL5 structure during the ion mobility experiment. But the ion mobility data do not provide sufficient information to delineate which aspects of the solution structure have changed and which aspects have been retained in the experiment. For example, the compaction of CCL5 could potentially result from the disordered N-terminal loop folding onto the Greek key motif, which means that the native residue-residue contacts of the Greek key could largely be retained. An alternative would be that the compaction could be caused by an overall re-folding of CCL5, in which case native residue-residue interactions would unlikely be retained. In the following, we apply the SRA method in conjunction with collisional-activated experiments to identify which aspects of the native structure are retained in the experiment and which are

3.2. Collision-induced unfolding measurements of CCL5 for non-reducing and reducing solution conditions

Fig. 2 shows the mass spectra for CCL5 recorded from aqueous and reducing conditions as described above. Both spectra show the same charge states (5+ to 11+) with similar abundances. Nevertheless, the isotopic patterns reveal that the two disulfide bonds remain intact under non-reducing aqueous conditions whereas they are both broken under reducing conditions (see Fig. S2, Supplementary Data). The corresponding ion mobility spectra are plotted in Fig. 3 and cross sections are tabulated in Table S1 (Supplementary Data).

The ion mobility spectra for charge states 5+ and 6+ from aqueous solution under "soft" conditions (Fig. 3A) resemble those recorded from ammonium acetate: the spectra exhibit one dominant feature at 1164 and 1225 Å², respectively, corresponding closely to the cross sections recorded from native conditions (1130 $Å^2$ and 1190 $Å^2$, see Fig. 1). Further, the peak widths are comparable and indicate presence of numerous, unresolved conformations. We note that, with the two disulfide bonds intact under non-reducing solution conditions, the cross sections and the peak widths remain essentially the same for charge states 5+ and 6+ even after collisional activation (Fig. 3B). By contrast, the spectra recorded for charge states 5+ and 6+ under reducing conditions exhibit two features (Fig. 3C). One feature (1138 ${\rm \AA}^2$ and 1213 ${\rm \AA}^2$ for charge states 5+ and 6+, respectively) is consistent in cross section with the feature observed under non-reducing conditions. The second feature, however, reflects more extended protein structures (1388 $\mbox{Å}^2$ and 1517 $\mbox{Å}^2$ for charge states 5+ and 6+, respectively). The collisional-activation experiments carried out for the reducing solution conditions demonstrate unfolding of the compact features to yield the extended feature (Fig. 3D).

For charge states 7+ to 11+, we observe more complex ion mobility spectra with multiple features present for both non-reducing and reducing solution conditions. The cross sections tend to increase with increasing charge state, with the spectra recorded under reducing conditions generally exhibiting more features with larger cross sections. Additionally, we notice a significant change in the number and the positions of peaks after collision-induced unfolding. These observations are overall consistent with prior reports and reflect the increased unfolding of the protein structures with higher charge states. This holds in particular for the reduced solution conditions where both disulfide bonds are broken.

3.3. Spectra predicted by the SRA method reproduce the overall trends observed in the ion mobility measurements

Fig. 4 compares the experimental ion mobility spectra to those predicted by the SRA for charge states 6+ to 9+. Fig. 4A and B

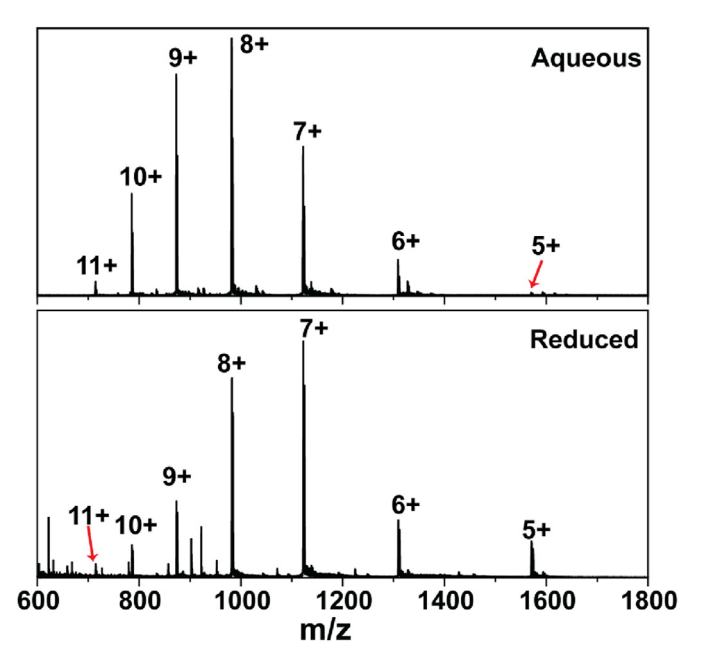


Fig. 2. Mass spectra recorded for aqueous and reduced CCL5 solutions. The same charge states (5+ to 11+) with similar relative abundance are obtained.

compare the measured and predicted spectra for the aqueous conditions for both "soft" and collisional-activating settings. We make several observations in the Figure. First, the SRA correctly predicts a compaction to occur for charge states 6+ and 7+ with respect to the NMR structure. This can be drawn from the observation that the predicted spectra for charge states 6+ and 7+ center at ~1220 Ų and ~1285 Ų, respectively, which is consistent with the experimental data (~1225 Ų and ~1333 Ų) but ~9–14 % smaller than the cross section expected for the NMR structure (1416 Ų). Second, the SRA correctly predicts that the mean of the abundances increases from approximately ~1200 Ų to ~1700 Ų when the charge state increases from 6+ to 9+. Further, the SRA correctly predicts the cross section to increase upon collisional activation. Hence, the data show that the SRA captures the essence of the unfolding process taking place in the "soft" ion mobility measurements for the various charge states.

The Pearson correlation coefficients ρ in Fig. 4A and B, however, also reveal discrepancies between the experimental data and the predictions made by the SRA. The coefficient ρ is 1.0 and 0.8 for charge states 6+ and 7+, but decreases to 0.3 and 0.1 for charge states 8+ and 9+, respectively. Indeed, the cross sections predicted by the SRA underestimate the experimental data by ~10-15 % for charge states 8+ and 9+ in Fig. 4A. Thus, the data indicate that the SRA overestimates the rigidity of the CCL5 structure for charge states 8+ and 9+ under "soft" settings. This discrepancy points to the notion that disulfide bonds could potentially break in the experiment after proton-migration to the disulfide bond [53,54]. Additionally, the data show that the fine structure of the SRA predictions deviates from those of the experiments. For example, the SRA does not recover the bimodal peak measured for charge state 8+ for "soft" settings from aqueous conditions in Fig. 4A. Moreover, the predicted peaks are typically broader than the experimentally measured peaks for "harsh" settings of higher charge states (7+ to 9+).

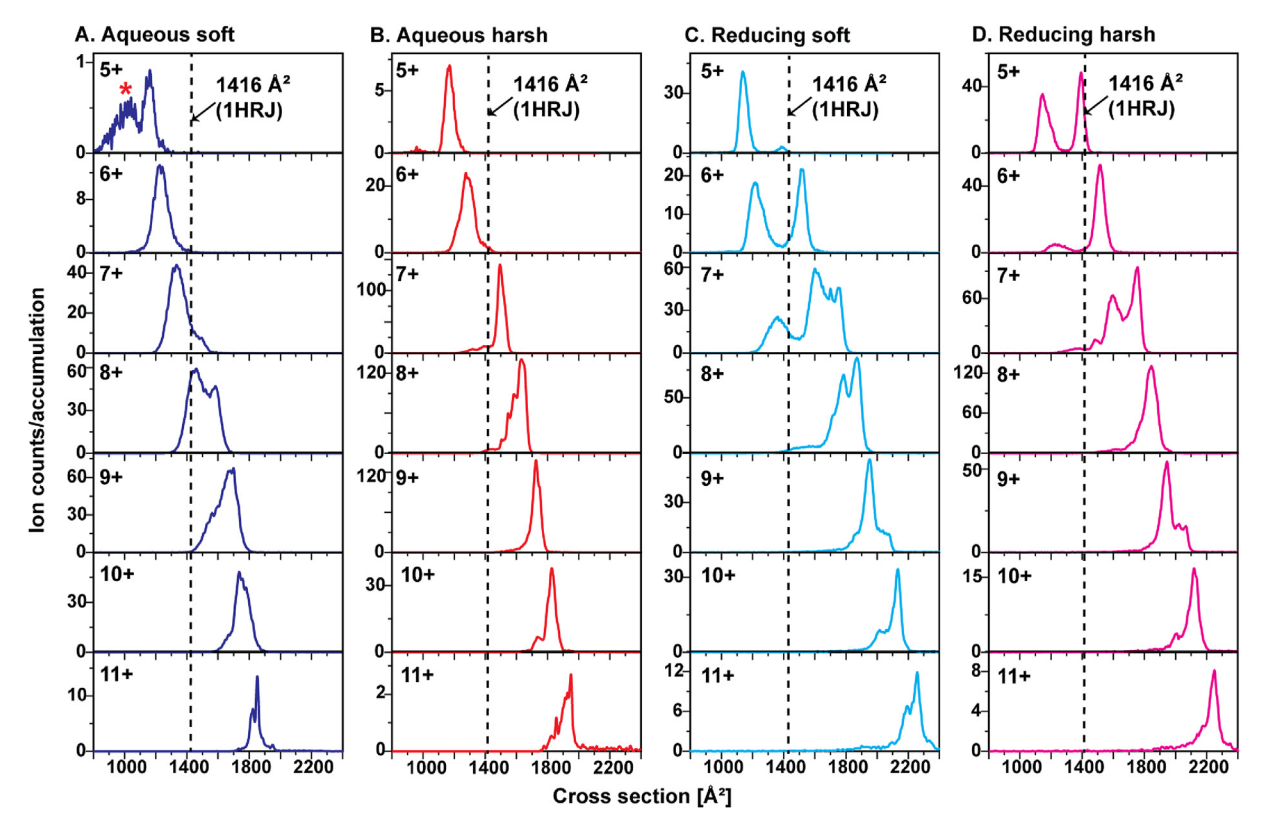


Fig. 3. Ion mobility spectra measured for CCL5. (A) Spectra recorded using "soft" TIMS settings for non-reducing, aqueous solution of CCL5 (blue trace). (B) Spectra recorded using "harsh" TIMS settings for non-reducing, aqueous solution conditions (red trace). (C) Spectra recorded using "soft" TIMS settings for reducing solution conditions (cyan trace). (D) Spectra recorded using "harsh" TIMS settings for reducing solution conditions of CCL5 (magenta trace). The dashed line indicates the cross section predicted by the PSA for the CCL5 NMR structure (PDB code: 1HRJ). Cross sections generally increase with charge state and with collisional-activation. The "soft" and "harsh" spectra for charge states 5+ and 6+ produced from non-reducing solution conditions agree with each other, indicating only minor structural changes of CCL5 after collisional-activation. Asterisk: noise.

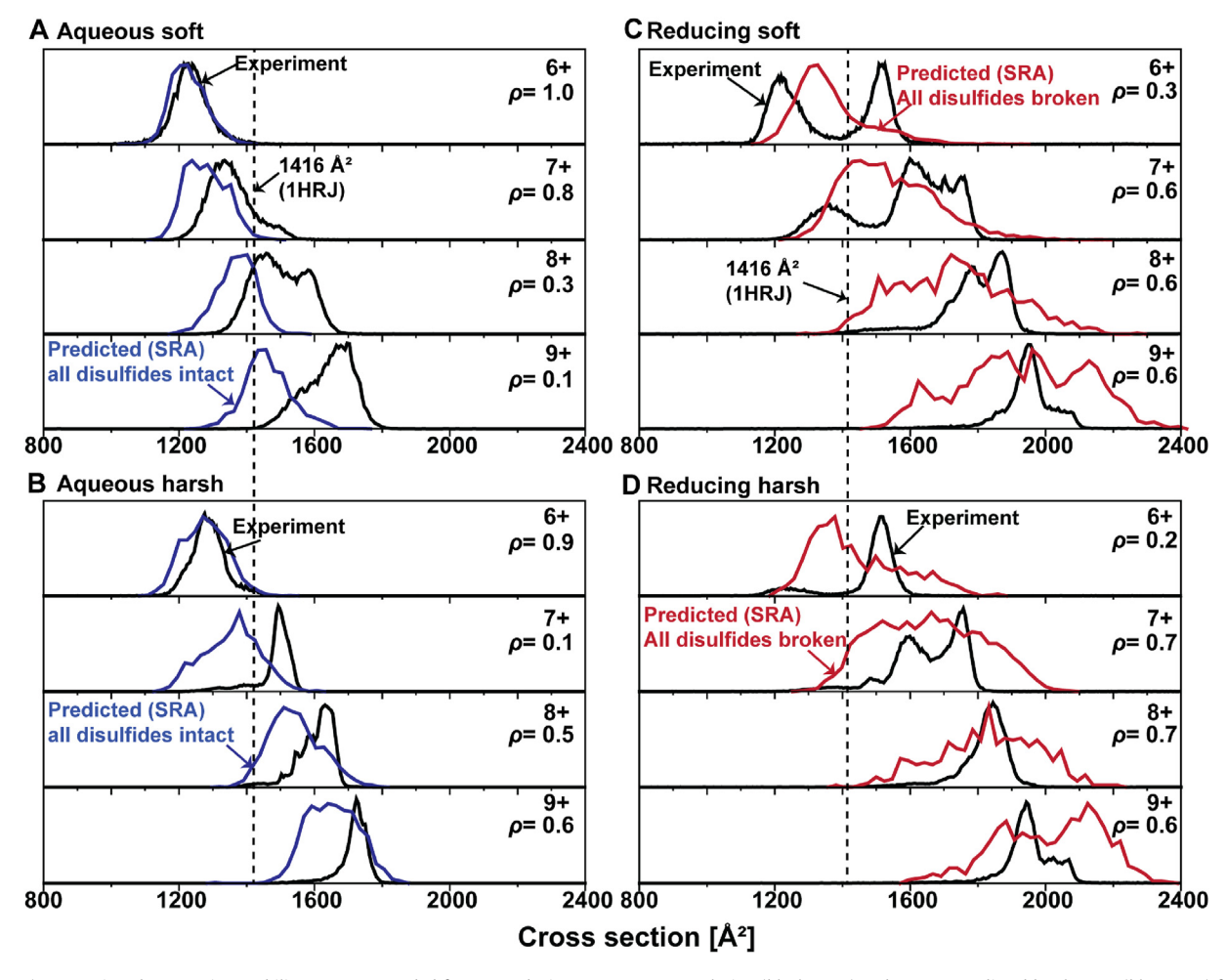


Fig. 4. (A, B) Comparison between ion mobility spectra recorded for non-reducing, aqueous CCL5 solution (black trace) and spectra predicted by the SRA (blue trace) for charge states 6+ to 9+ ions in nitrogen buffer gas. The two disulfide bonds are kept intact in SRA. The trend of unfolding as the increase of charge is successfully probed by SRA for both "soft" (A) and "harsh" (B) conditions. However, the shape of ion mobility spectra has not been accurately recovered by SRA. (C,D) Comparison between ion mobility spectra recorded for reducing CCL5 solution (black trace) and spectra predicted by the SRA (red trace) for charge states 6+ to 9+ ions in nitrogen buffer gas. The two disulfide bonds are kept broken in SRA. The data indicate that the SRA correctly predicts the compaction of charge states 6+ and 7+ and the overall trends of the unfolding with increasing charge state. The dashed line indicates the cross section predicted by the PSA for the CCL5 NMR structure (PDB code: 1HRJ). Pearson correlation coefficients ρ indicate the similarity between the experimental and predicted ion mobility spectra.

We make similar observations in Fig. 4C and D, which compare ion mobility spectra recorded for the reducing solution conditions to the corresponding SRA predictions (with all disulfide bonds broken). The data shown in Fig. 4C and D reveal that the SRA predictions recover the overall trends in the experimental data when going from charge state 6+ to 9+ for both the "soft" and the collisional-activated spectra. That is, the SRA correctly predicts the abundances to increase from approximately ~1200 Å² to ~2000 Å² for charge states 6+ to 9+. The predicted peak widths, however, are significantly broader than the experimental peaks, especially for the collisional-activated spectra and the higher charge states. This discrepancy is also reflected by correlation coefficients on the order of 0.6–0.7 for all but charge state 6+ in Fig. 4C and D. Additionally, the predictions do not accurately recover the fine structure of the peaks. For example, the SRA predicts a broad feature for charge states 6+ and 7+ under soft settings (Fig. 4C) with maximum abundance in-between the positions of the experimental peaks.

Overall, the observations made above are in line with our observations made previously for the protein ubiquitin: the SRA succeeds in describing the main trends of the unfolding process for the protein in the gas phase. The Pearson correlation coefficients ρ indicate that the SRA predictions here agree reasonably well with

the experiment for native conditions and low charge states as well as for reduced conditions and high charge states. By contrast, discrepancies are observed for high charge states obtained from native conditions and for low charge states obtained from reducing conditions. These discrepancies observed between the experimental and predicted spectra indicate that the SRA method does not yet succeed in modelling the details of the structural transitions occurring in the ion mobility experiment for all combinations of experimental conditions and charge states. This discrepancy likely stems from the fact that currently available force fields do not allow for appropriate modeling of proton transfer processes, and other chemical reactions, taking place in the experiment. The two key shortcomings with the current state of affairs are: (1) currently available force fields are optimized for solution simulations and (2) allow only the side chains of amino acids to be protonated or deprotonated; (3) standard molecular dynamics packages do not allow for changes in the bonding during the simulation. By contrast, it is well-known from the proton mobile model and the pathways in competition model of collision-induced dissociation of peptides that the extra protons sample the carbonyl oxygen and amide nitrogen atoms of the peptide bonds [55,56]. Indeed, Konermann et al. [57] reported on the significance of accounting for mobile

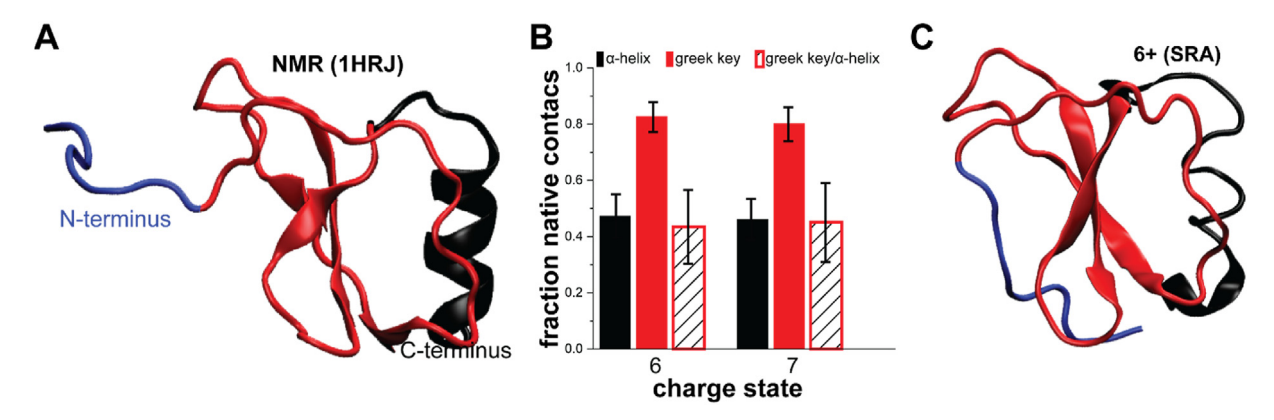


Fig. 5. (A) NMR structure of CCL5 with unstructured N-terminal loop, the central region comprising the Greek key motif, and the C-terminal α -helix indicated. (B) Fraction of native contacts Q calculated for the structures predicted by the SRA method for charge states 6+ and 7+ for aqueous, "soft" conditions (see Fig. 4A). (C) CCL5 structure illustrating the retention of native residue-residue interactions for charge state 6+.

protons in molecular dynamics simulations due to proton mobility reducing the stability of salt bridges, thereby effecting the stability of peptides and proteins in the gas phase. Hence, the discussion here suggests that accurately treating proton transfer processes during the gas phase relaxation process would significantly enhance the fidelity of the predictions made by the SRA.

3.4. Compaction of CCL5 in the ion mobility experiment

The discussion above revealed that CCL5 undergoes a significant compaction during the ion mobility spectrometry/mass spectrometry experiment. This compaction is indicated by the fact that the cross sections measured for the charge states 5+ and 6+ under native and aqueous conditions are significantly lower than the cross sections expected for the NMR structure of CCL5 (see Figs. 1 and 3). Further, the discussion above showed that the SRA correctly predicts the compaction of the CCL5 structure as well as the overall trends in the experimental ion mobility spectra. In this section we thus discuss the compaction of CCL5 on the basis of the SRA calculations: what aspects of the solution structure are retained, and what aspects are not retained, in the experiment?

Fig. 5A shows the NMR structure of CCL5 with color-coding of the unstructured N-terminal loop, the central region comprising the Greek key motif, and the C-terminal α -helix. To identify the extent to which the native structure is retained in the ion mobility experiments, we followed our prior approach [16] and calculated the fraction of native contacts Q for the structures predicted by the SRA for charge states 6+ and 7+ (see Fig. 5B). The analysis indicates that the central region with the Greek key is strongly retained $(0 \ge 0.8)$. Further, the data indicate that approximately half of the native contacts within the C-terminal α -helix are retained as are the contacts between the central region and the C-terminal α -helix. The N-terminal region remains unstructured and tends to fold onto the central region containing the Greek key. We illustrate the retention of native contacts by the representative structure (taken as the central structure of the most abundant structural ensemble) for charge state 6+ in Fig. 5C. Overall, the SRA predicts that the significant compaction observed for the CCL5 structure in the ion mobility measurement is caused mainly by the disordered N-terminal loop folding onto the Greek key motif of CCL5, while the native residue-residue contacts within the Greek key motif and Cterminal α -helix are retained to a significant extent. These findings are consistent with prior work [23] in that protein ions compact upon solvent-removal while largely retaining α -helices and β sheets present in the native state.

4. Summary and conclusions

We recorded ion mobility spectra for various charge states and solution conditions of the human CCL5. Comparison of the measured cross sections to the NMR structure (PDB:1HRJ) revealed that CCL5 undergoes a significant compaction under native mass spectrometry conditions. We applied the Structure Relaxation Approximation (SRA) method to identify which aspects of the native solution structure are retained in the ion mobility measurement, and which aspects are not retained.

Our data show that the SRA predictions reproduce the overall trends in the experimental ion mobility spectra: the SRA correctly predicts (1) the compaction of the CCL5 structure as seen in the experiments; and (2) the general increase in the cross section for the various charge states. The SRA attributes the compaction of the CCL5 structure mainly to the folding of the unstructured loop of CCL5 onto the central Greek key motif. By contrast, the SRA indicates that the native residue-residue contacts present in the NMR structure are retained to a significant extent in these two regions. Nevertheless, our analysis also indicates accurately treating proton transfer processes would significantly improve the structural interpretation of ion mobility data by the SRA.

Author contributions

All authors conceived and analyzed the experiments and calculations. M.C. performed the measurements and calculations. The manuscript was written through contributions of all authors.

Declaration of competing interest

The authors declare that they have no known competing financial interests or personal relationships that could have appeared to influence the work reported in this paper.

Acknowledgement

This work was supported by the National Science Foundation under grant CHE-1654608 (C.B.). C.B. acknowledges support from the FSU Council on Research & Creativity.

Appendix A. Supplementary data

Supplementary data to this article can be found online at https://doi.org/10.1016/j.ijms.2021.116682.

References

- [1] C.V. Robinson, A. Sali, W. Baumeister, The molecular sociology of the cell, Nature 450 (2007) 973–982, https://doi.org/10.1038/nature06523.
- [2] D.E. Clemmer, D.H. Russell, E.R. Williams, Characterizing the conformationome: toward a structural understanding of the proteome, Acc. Chem. Res. 50 (2017) 556–560, https://doi.org/10.1021/acs.accounts.6b00548.
- [3] Y. Cai, J. Zhang, T. Xiao, H. Peng, S.M. Sterling, R.M. Walsh, S. Rawson, S. Rits-Volloch, B. Chen, Distinct conformational states of SARS-CoV-2 spike protein, Science 369 (2020) 1586–1592, https://doi.org/10.1126/science.abd4251.
- [4] E. Hubin, N.A.J. van Nuland, K. Broersen, K. Pauwels, Transient dynamics of Aβ contribute to toxicity in Alzheimer's disease, Cell. Mol. Life Sci. 71 (2014) 3507–3521, https://doi.org/10.1007/s00018-014-1634-z.
- [5] L.M. Smith, N.L. Kelleher, Proteoforms as the next proteomics currency, Science 359 (2018) 1106–1107, https://doi.org/10.1126/science.aat1884.
- [6] Y. Watanabe, J.D. Allen, D. Wrapp, J.S. McLellan, M. Crispin, Site-specific glycan analysis of the SARS-CoV-2 spike, Science 369 (2020) 330–333, https:// doi.org/10.1126/science.abb9983.
- [7] L.M. Miller, L.F. Barnes, S.A. Raab, B.E. Draper, T.J. El-Baba, C.A. Lutomski, C.V. Robinson, D.E. Clemmer, M.F. Jarrold, Heterogeneity of glycan processing on trimeric SARS-CoV-2 spike protein revealed by charge detection mass spectrometry, J. Am. Chem. Soc. 143 (2021) 3959—3966, https://doi.org/ 10.1021/jacs.1c00353.
- [8] D.P. Smith, S.E. Radford, A.E. Ashcroft, Elongated oligomers in β2-microglobulin amyloid assembly revealed by ion mobility spectrometry-mass spectrometry, Proc. Natl. Acad. Sci. Unit. States Am. 107 (2010) 6794–6798, https://doi.org/10.1073/pnas.0913046107.
- [9] L.M. Young, P. Cao, D.P. Raleigh, A.E. Ashcroft, S.E. Radford, Ion mobility spectrometry—mass spectrometry defines the oligomeric intermediates in amylin amyloid formation and the mode of action of inhibitors, J. Am. Chem. Soc. 136 (2014) 660–670, https://doi.org/10.1021/ja406831n.
- [10] D. Wu, W.B. Struwe, D.J. Harvey, M.A.J. Ferguson, C.V. Robinson, N-glycan microheterogeneity regulates interactions of plasma proteins, Proc. Natl. Acad. Sci. Unit. States Am. 115 (2018) 8763–8768, https://doi.org/10.1073/ pnas.1807439115.
- [11] F.C. Liu, T.C. Cropley, M.E. Ridgeway, M.A. Park, C. Bleiholder, Structural analysis of the glycoprotein complex avidin by tandem-trapped ion mobility spectrometry—mass spectrometry (Tandem-TIMS/MS), Anal. Chem. 92 (2020) 4459—4467, https://doi.org/10.1021/acs.analchem.9b05481.
- [12] A. McPherson, J.A. Gavira, Introduction to protein crystallization, Acta Crystallogr. Sect. F Struct. Biol. Commun. 70 (2013) 2–20, https://doi.org/10.1107/S2053230X13033141.
- [13] K. Wuthrich, Protein structure determination in solution by nuclear magnetic resonance spectroscopy, Science 243 (1989) 45–50, https://doi.org/10.1126/ science.2911719.
- [14] T. Wyttenbach, M.T. Bowers, Structural stability from solution to the gas phase: native solution structure of ubiquitin survives analysis in a solvent-free ion mobility—mass spectrometry environment, J. Phys. Chem. B 115 (2011) 12266–12275, https://doi.org/10.1021/jp206867a.
- [15] T. Wyttenbach, N.A. Pierson, D.E. Clemmer, M.T. Bowers, Ion mobility analysis of molecular dynamics, Annu. Rev. Phys. Chem. 65 (2014) 175–196, https:// doi.org/10.1146/annurev-physchem-040513-103644.
- [16] C. Bleiholder, F.C. Liu, Structure relaxation approximation (SRA) for elucidation of protein structures from ion mobility measurements, J. Phys. Chem. B 123 (2019) 2756–2769, https://doi.org/10.1021/acs.jpcb.8b11818.
- [17] C.J. Hogan, B.T. Ruotolo, C.V. Robinson, J. Fernandez de la Mora, Tandem differential mobility analysis-mass spectrometry reveals partial gas-phase collapse of the GroEL complex, J. Phys. Chem. B 115 (2011) 3614–3621, https://doi.org/10.1021/jp109172k.
- [18] M. Jenner, J. Ellis, W.-C. Huang, E. Lloyd Raven, G.C.K. Roberts, N.J. Oldham, Detection of a protein conformational equilibrium by electrospray ionisationion mobility-mass spectrometry, Angew. Chem. Int. Ed. 50 (2011) 8291–8294, https://doi.org/10.1002/anie.201101077.
- [19] E. Jurneczko, P.E. Barran, How useful is ion mobility mass spectrometry for structural biology? The relationship between protein crystal structures and their collision cross sections in the gas phase, Analyst 136 (2011) 20–28, https://doi.org/10.1039/C0AN00373E.
- [20] I.D.G. Campuzano, C. Larriba, D. Bagal, P.D. Schnier, Ion mobility and mass spectrometry measurements of the humanized IgGk NIST monoclonal antibody, in: State—Art Emerg. Technol. Ther. Monoclon. Antib. Charact. Vol. 3 Defin. Gener. Anal. Biophys. Tech., American Chemical Society, 2015, pp. 75—112, https://doi.org/10.1021/bk-2015-1202.ch004.
- [21] F. Debaene, A. Bœuf, E. Wagner-Rousset, O. Colas, D. Ayoub, N. Corvaïa, A. Van Dorsselaer, A. Beck, S. Cianférani, Innovative native MS methodologies for antibody drug conjugate characterization: high resolution native MS and IM-MS for average DAR and DAR distribution assessment, Anal. Chem. 86 (2014) 10674–10683, https://doi.org/10.1021/ac502593n.
- [22] K.J. Pacholarz, M. Porrini, R.A. Garlish, R.J. Burnley, R.J. Taylor, A.J. Henry, P.E. Barran, Dynamics of intact immunoglobulin G explored by drift-tube ionmobility mass spectrometry and molecular modeling, Angew. Chem. Int. Ed. 53 (2014) 7765–7769, https://doi.org/10.1002/anie.201402863.
- [23] A.D. Rolland, J.S. Prell, Computational insights into compaction of gas-phase protein and protein complex ions in native ion mobility-mass spectrometry, TrAC Trends Anal. Chem. 116 (2019) 282–291, https://doi.org/10.1016/

j.trac.2019.04.023.

- [24] P.W.A. Devine, H.C. Fisher, A.N. Calabrese, F. Whelan, D.R. Higazi, J.R. Potts, D.C. Lowe, S.E. Radford, A.E. Ashcroft, Investigating the structural compaction of biomolecules upon transition to the gas-phase using ESI-TWIMS-MS, J. Am. Soc. Mass Spectrom. 28 (2017) 1855–1862, https://doi.org/10.1007/s13361-017-1689-9
- [25] F.C. Liu, M.E. Ridgeway, M.A. Park, C. Bleiholder, Tandem trapped ion mobility spectrometry, Analyst 143 (2018) 2249–2258, https://doi.org/10.1039/ C7AN02054F
- [26] S.R. Kirk, F.C. Liu, T.C. Cropley, H.R. Carlock, C. Bleiholder, On the preservation of non-covalent peptide assemblies in a tandem-trapped ion mobility spectrometer-mass spectrometer (TIMS-TIMS-MS), J. Am. Soc. Mass Spectrom. 30 (2019) 1204–1212, https://doi.org/10.1007/s13361-019-02200-y.
- [27] K.J. Laszlo, E.B. Munger, M.F. Bush, Folding of protein ions in the gas phase after cation-to-anion proton-transfer reactions, J. Am. Chem. Soc. 138 (2016) 9581–9588, https://doi.org/10.1021/jacs.6b04282.
- [28] J.D. Eschweiler, R.M. Martini, B.T. Ruotolo, Chemical probes and engineered constructs reveal a detailed unfolding mechanism for a solvent-free multidomain protein, J. Am. Chem. Soc. 139 (2017) 534–540, https://doi.org/ 10.1021/jacs.6b11678.
- [29] S.M. Dixit, D.A. Polasky, B.T. Ruotolo, Collision induced unfolding of isolated proteins in the gas phase: past, present, and future, Curr. Opin. Chem. Biol. 42 (2018) 93–100, https://doi.org/10.1016/j.cbpa.2017.11.010.
- [30] D. Rossi, A. Zlotnik, The biology of chemokines and their receptors, Annu. Rev. Immunol. 18 (2000) 217–242.
- [31] V. Appay, S.L. Rowland-Jones, RANTES: a versatile and controversial chemokine, Trends Immunol. 22 (2001) 83–87.
- [32] T.J. Schall, Biology of the RANTES/SIS cytokine family, Cytokine 3 (1991) 165–183.
- [33] A.J. Vila-Coro, M. Mellado, A.M. de Ana, C. Martínez-A, J.M. Rodríguez-Frade, Characterization of RANTES- and aminooxypentane-RANTES- triggered desensitization signals reveals differences in recruitment of the G protein-coupled receptor complex, J. Immunol. 163 (1999) 3037–3044.
- [34] M. Wiktor, O. Hartley, S. Grzesiek, Characterization of structure, dynamics, and detergent interactions of the anti-HIV chemokine variant 5P12-RANTES, Biophys. J. 105 (2013) 2586–2597, https://doi.org/10.1016/j.bpj.2013.10.025.
- [35] F. Cocchi, A.L. DeVico, A. Garzino-Demo, S.K. Arya, R.C. Gallo, P. Lusso, Identification of RANTES, MIP-1α, and MIP-1β as the major HIV-suppressive factors produced by CD8+ T cells, Science 270 (1995) 1811–1815, https://doi.org/10.1126/science.270.5243.1811.
- [36] M. Scigelova, P.S. Green, A.E. Giannakopulos, A. Rodger, D.H. Crout, P.J. Derrick, A practical protocol for the reduction of disulfide bonds in proteins prior to analysis by mass spectrometry, Eur. J. Mass Spectrom. 7 (2001) 29–34.
- [37] D.R. Hernandez, J.D. DeBord, M.E. Ridgeway, D.A. Kaplan, M.A. Park, F. Fernandez-Lima, Ion dynamics in a trapped ion mobility spectrometer, Analyst 139 (2014) 1913–1921, https://doi.org/10.1039/C3AN02174B.
- [38] K. Michelmann, J.A. Silveira, M.E. Ridgeway, M.A. Park, Fundamentals of trapped ion mobility spectrometry, J. Am. Soc. Mass Spectrom. 26 (2015) 14–24, https://doi.org/10.1007/s13361-014-0999-4.
- [39] F.C. Liu, S.R. Kirk, C. Bleiholder, On the structural denaturation of biological analytes in trapped ion mobility spectrometry – mass spectrometry, Analyst 141 (2016) 3722–3730, https://doi.org/10.1039/C5AN02399H.
- [40] F.C. Liu, S.R. Kirk, C. Bleiholder, On the structural denaturation of biological analytes in trapped ion mobility spectrometry – mass spectrometry, Analyst 141 (2016) 3722–3730, https://doi.org/10.1039/C5AN02399H.
- [41] M.E. Ridgeway, J.A. Silveira, J.E. Meier, M.A. Park, Microheterogeneity within conformational states of ubiquitin revealed by high resolution trapped ion mobility spectrometry, Analyst 140 (2015) 6964–6972, https://doi.org/ 10.1039/C5AN00841G.
- [42] M. Chai, M.N. Young, F.C. Liu, C. Bleiholder, A. Transferable, Sample-independent calibration procedure for trapped ion mobility spectrometry (TIMS), Anal. Chem. 90 (2018) 9040–9047, https://doi.org/10.1021/acs.analchem.8b01326.
- [43] D.R. Hernandez, J.D. DeBord, M.E. Ridgeway, D.A. Kaplan, M.A. Park, F. Fernandez-Lima, Ion dynamics in a trapped ion mobility spectrometer, Analyst 139 (2014) 1913–1921, https://doi.org/10.1039/c3an02174b.
- [44] J.A. Silveira, M.E. Ridgeway, M.A. Park, High resolution trapped ion mobility spectrometery of peptides, Anal. Chem. 86 (2014) 5624–5627, https://doi.org/ 10.1021/ac501261h.
- [45] S.M. Stow, T.J. Causon, X. Zheng, R.T. Kurulugama, T. Mairinger, J.C. May, E.E. Rennie, E.S. Baker, R.D. Smith, J.A. McLean, S. Hann, J.C. Fjeldsted, An interlaboratory evaluation of drift tube ion mobility—mass spectrometry collision cross section measurements, Anal. Chem. 89 (2017) 9048–9055, https://doi.org/10.1021/acs.analchem.7b01729.
- [46] C.-W. Chung, R.M. Cooke, A.E. Proudfoot, T.N. Wells, The three-dimensional solution structure of RANTES, Biochemistry 34 (1995) 9307–9314.
- [47] H.J.C. Berendsen, D. van der Spoel, R. van Drunen, GROMACS: a messagepassing parallel molecular dynamics implementation, Comput. Phys. Commun. 91 (1995) 43–56, https://doi.org/10.1016/0010-4655(95)00042-E.
- [48] Y. Duan, C. Wu, S. Chowdhury, M.C. Lee, G. Xiong, W. Zhang, R. Yang, P. Cieplak, R. Luo, T. Lee, J. Caldwell, J. Wang, P. Kollman, A point-charge force field for molecular mechanics simulations of proteins based on condensed-phase quantum mechanical calculations, J. Comput. Chem. 24 (2003) 1999–2012, https://doi.org/10.1002/jcc.10349.
- [49] C. Bleiholder, T. Wyttenbach, M.T. Bowers, A novel projection approximation

- algorithm for the fast and accurate computation of molecular collision cross sections (I). Method, Int. J. Mass Spectrom. 308 (2011) 1–10, https://doi.org/ 10.1016/j.ijms.2011.06.014.
- [50] S.E. Anderson, C. Bleiholder, E.R. Brocker, P.J. Stang, M.T. Bowers, A novel projection approximation algorithm for the fast and accurate computation of molecular collision cross sections (III): application to supramolecular coordination-driven assemblies with complex shapes, Int. J. Mass Spectrom. (2012) 330–332, https://doi.org/10.1016/j.ijms.2012.08.024, 78–84.
- [51] C. Bleiholder, S. Contreras, T.D. Do. M.T. Bowers, A novel projection approximation algorithm for the fast and accurate computation of molecular collision cross sections (II). Model parameterization and definition of empirical shape factors for proteins, Int. J. Mass Spectrom. (2013) 345–347, https://doi.org/ 10.1016/j.ijms.2012.08.027, 89–96.
- [52] C. Bleiholder, S. Contreras, M.T. Bowers, A novel projection approximation algorithm for the fast and accurate computation of molecular collision cross sections (IV). Application to polypeptides, Int. J. Mass Spectrom. (2013) 354–355, https://doi.org/10.1016/j.ijms.2013.06.011, 275–280. [53] J.M. Wells, J.L. Stephenson, S.A. McLuckey, Charge dependence of protonated

- insulin decompositions, Int. J. Mass Spectrom. 203 (2000) A1-A9, https:// doi.org/10.1016/S1387-3806(00)00389-4.
- H. Lioe, R.A.J. OrsHair, A novel salt bridge mechanism highlights the need for nonmobile proton conditions to promote disulfide bond cleavage in protonated peptides under low-energy collisional activation, J. Am. Soc. Mass Spectrom. 18 (2007) 1109—1123, https://doi.org/10.1016/jj.jasms.2007.03.003.
- A.R. Dongre, J.L. Jones, Á. Somogyi, V.H. Wysocki, Influence of peptide composition, gas-phase basicity, and chemical modification on fragmentation efficiency: evidence for the mobile proton model, J. Am. Chem. Soc. 118 (1996)
- [56] C. Bleiholder, S. Osburn, T.D. Williams, S. Suhai, M. Van Stipdonk, A.G. Harrison, B. Paizs, Sequence-scrambling fragmentation pathways of protonated peptides, J. Am. Chem. Soc. 130 (2008) 17774-17789, https:// doi.org/10.1021/ia805074d.
- L. Konermann, E. Aliyari, J.H. Lee, Mobile protons limit the stability of salt bridges in the gas phase: implications for the structures of electrospraved protein ions, J. Phys. Chem. B 125 (2021) 3803–3814, https://doi.org/10.1021/ acs.ipcb.1c00944.